*Journal of Biophotonics*

JOURNAL OF BIOPHOTONICS

RESEARCH ARTICLE OPEN ACCESS

# Necrotizing Enterocolitis Detection in Premature Infants Using Broadband Optical Spectroscopy

Ethan Flowerday[1] | Ali Daneshkhah[1] | Yuanzhe Su[1] | Vadim Backman[1] | Seth D. Goldstein[2,3]

[1]Department of Biomedical Engineering, Northwestern University, Evanston, Illinois, USA | [2]Department of Surgery, Northwestern School of Medicine, Chicago, Illinois, USA | [3]Division of Pediatric Surgery, Lurie Children's Hospital, Chicago, Illinois, USA

**Correspondence:** Seth D. Goldstein (seth.goldstein@northwestern.edu)

**Received:** 19 June 2024 | **Revised:** 15 October 2024 | **Accepted:** 16 October 2024

**Funding:** This work was supported by The Gerber Foundation. Additional support made possible by the National Institutes of Health Grants (NIH) grants U54CA268084, R01CA228272, and R01CA225002, National Science Foundation grant (NSF) Grant EFMA-1830961, and philanthropic support from Rob and Kristin Goldman and the Christina Carinato Charitable Foundation.

**Keywords:** deep learning | diagnosis | machine learning | neonatal diseases | spectroscopy

## ABSTRACT

Necrotizing enterocolitis (NEC) is a devastating disease affecting premature infants. Broadband optical spectroscopy (BOS) is a method of noninvasive optical data collection from intra-abdominal organs in premature infants, offering potential for disease detection. Herein, a novel machine learning approach, iterative principal component analysis (iPCA), is developed to select optimal wavelengths from BOS data collected in vivo from neonatal intensive care unit (NICU) patients for NEC classification. Neural network models were trained for classification, with a reduced-feature model distinguishing NEC with an accuracy of 88%, a sensitivity of 89%, and a specificity of 88%. While whole-spectrum models performed the best for accuracy and specificity, a reduced feature model excelled in sensitivity, with minimal cost to other metrics. This research supports the hypothesis that the analysis of human tissue via BOS may permit noninvasive disease detection. Furthermore, a medical device optimized with these models may potentially screen for NEC with as few as seven wavelengths.

## 1 | Introduction

Necrotizing enterocolitis (NEC) is a devastating disease of premature infants, with mortality rates as high as 50% [1]. Although the mechanism is not fully characterized nor understood, the disorder ultimately leads to ischemia and necrosis of the colon and small intestines in affected infants [2]. At its most severe, this requires surgical resection of the affected bowel and numerous downstream consequences for these fragile neonates. Notably, early detection of and timely medical intervention for NEC may hopefully prevent progression and avoid the need for life-saving emergent operations [3–5]. Thus, there is a pressing clinical need for the development of a noninvasive, accessible, and accurate approach for objective identification of NEC.

Recognition of NEC is often challenging due to a lack of objective signs and symptoms. Serum biomarkers are nonspecific, and imaging revolves around identifying tissue damage after the fact. However, surgeons have long recognized that there is a characteristic appearance of threatened bowel at the time of laparotomy. The cellular byproducts of ischemia are dark chromophores; accordingly, it is hypothesized that there is a noninvasive spectroscopic approach that has potential to identify NEC. Optical spectroscopy has shown promise in characterizing biological tissues, often described as a future alternative to

**Abbreviations:** AUC, area under the curve; BOS, Broadband optical spectroscopy; iPCA, iterative principal component analysis; NEC, necrotizing enterocolitis; NICU, neonatal intensive care unit; NIR, near-infrared; PCA, principal component analysis; ReLu, rectified linear unit.

biopsy [6, 7]. In the context of this promise, and the very thin abdominal wall of infants at risk for NEC, we have endeavored to explore the use of broadband optical spectroscopy (BOS) as a novel point-of-care technology. Unlike quantitative spectroscopy methods such as tissue oximeters, which target oxyhemoglobin as an individual chromophore [8], BOS is tailored to reveal qualitative variations between tissues. It has been shown that wavelengths up to 1000 nm can penetrate up to 5 mm in tissue, with higher wavelength near-infrared (NIR) optical windows expected to achieving even greater penetration [9, 10]. This is sufficient to pass the skin (< 1.5 mm) [11–13], reaching the underlying tissue of the abdomen. This has been demonstrated previously in an animal model of NEC but has not yet been analyzed in humans [14].

Without a fully known molecular mechanism, the discriminatory ability of BOS for NEC rests on advanced signal processing techniques. An empirical approach is mandatory, as tissue samples for biochemical correlation are neither practical nor available. In this manuscript we report the development of a deep learning technique for BOS data. First, a neural network was built and trained on sample readings labeled as either unaffected or diseased, resulting in a classification accuracy of approximately 90%. Then, an iterative principal component analysis (iPCA) characterized local extrema and selected a panel of synergetic features. Previously, the effectiveness of this machine learning approach was demonstrated in tissue classification [15]. In this study, we further validate it through clinical data analysis. Finally, new neural networks were trained using the iPCA selected features in order to ascertain the future feasibility of a lower-fidelity spectrum, showing a minimal trade-off in model metrics compared to the whole-spectrum trained model.

## 2 | Materials and Methods

### 2.1 | Patient Recruitment and Data Collection

Infants were enrolled by voluntary parental consent in a Northwestern University Institutional Review Board-approved study across two academic neonatal intensive care units (NICUs). Inclusion criteria required infants to have a corrected gestational age of less than 36 weeks. Subjects were excluded for congenital cardiac anomalies, known abdominal organ diseases, or prior abdominal surgeries. Once enrolled, infants underwent daily measurements of their abdomen up to a corrected gestational age of 36 weeks. Abdominal readings were performed in three distinct areas; right lower quadrant, left lower quadrant, and suprapubic region.

BOS measurements were obtained using a handheld probe with a broad-spectrum light source coupled to a laboratory grade spectrometer (ASD LabSpec 4, Malvern Panalytical), with a detection range of 350–2500 nm, thus covering both the visible and NIR ranges. The captured data entailed a 100–500-fold increase in spectral resolution granularity beyond commercially available NIR oximeters [16]. Calibration to a Spectralon reference panel (Malvern Panalytical) was performed prior to each measurement. Data collection does not cause discomfort and there is no known or theorized harm related to BOS, which requires only a gentle touch on the baby's skin for under 1 s with no ionizing radiation. The handheld probe was placed in contact with the area of interest to reduce ambient light, as seen in Figure 1.

Measurements were taken in duplicate for each region of interest on 89 patients, resulting in 11 570 spectral scans. Using clinician categorization, 11 367 spectra from 89 patients were categorized as normal, and 203 spectra from 14 patients were categorized as NEC. Raw data from a single patient are displayed in Figure 2, with healthy and diseased spectra indicated. The occurrence of NEC was determined by a surgeon blinded to the research analysis conducted. As NEC is not a single pathophysiological entity but rather a multifactorial condition, the characterization of data in this study was determined by a patient's physician. A retrospective review of bedside clinician impressions, hemodynamics, imaging findings, and clinical course was performed. Generally, pneumatosis or portal venous gas on radiograph in addition to any of the following led to a diagnosis of NEC: bloody bowel movement, abdominal distention, sepsis hemodynamics. Only BOS readings taken within 24 h of activate NEC suspicion on radiographs were labelled as diseased. Preprocessing included truncation to a range of 400–2400 nm due to noise and relatively low intensity illumination at the periphery of the spectrum, followed by min/max normalization based on the spectral intensity.

### 2.2 | Training of Neural Network Models

The spectral data were randomly partitioned into a 75% training data and 25% validation data split. For training, the prevalence

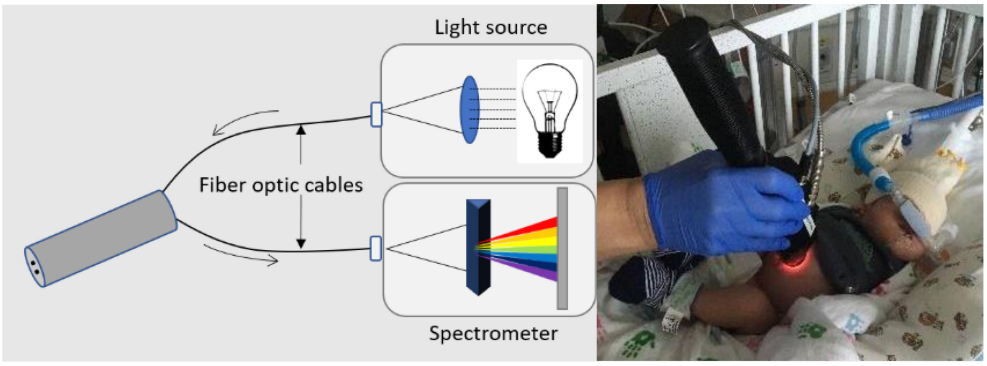


**FIGURE 1** | (left) Schematic of optical system; (right) capturing an abdominal reading from a subject.

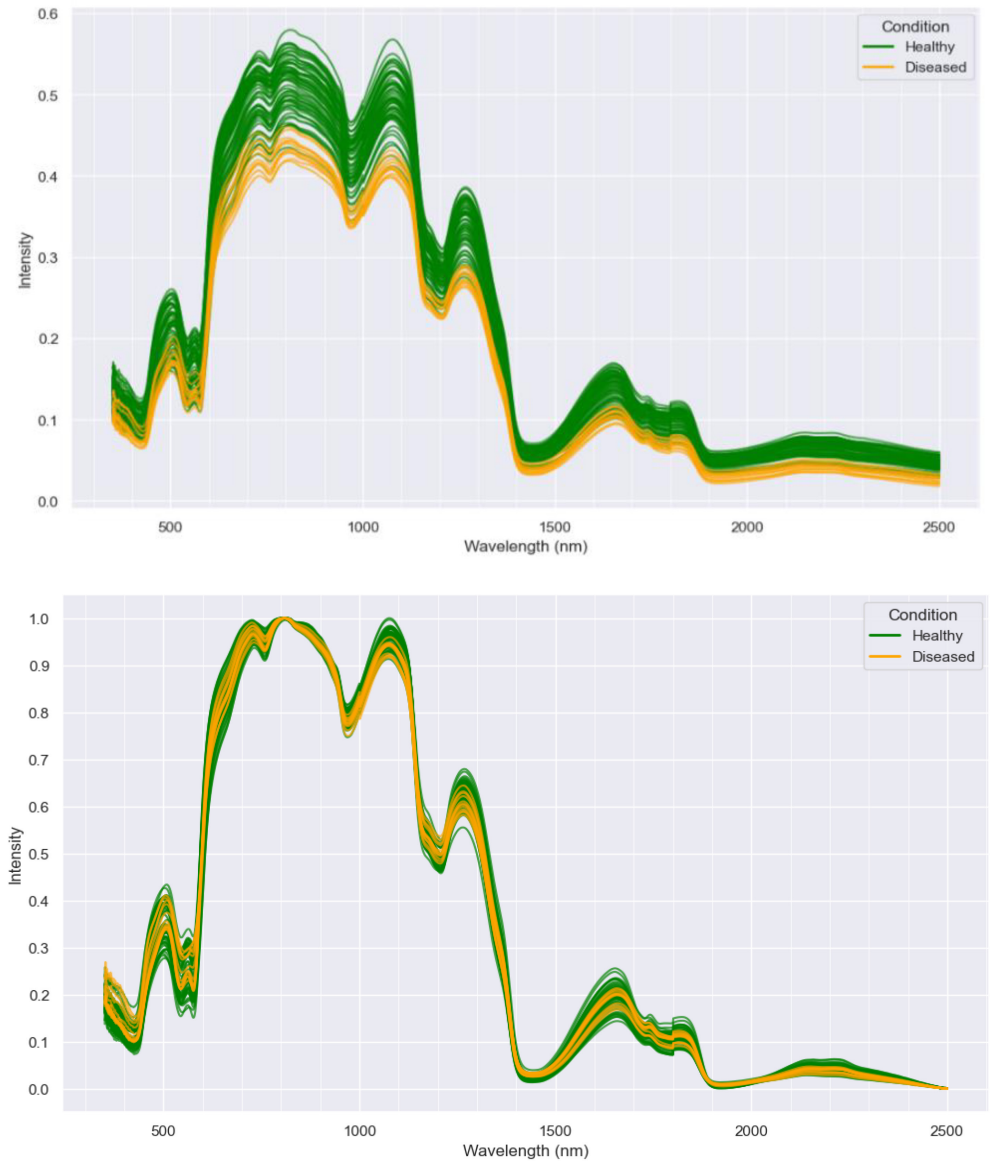


**FIGURE 2** | Data plotted from a single patient with healthy spectra displayed in green and diseased spectra displayed in orange. (top) Raw data and (bottom) scaled data.

of NEC labelled data was increased to comprise 50% of the training data through random sampling with replacement. This was done to prevent the models from overfitting to healthy labelled spectra due to the label imbalance in the data. For the validation data, the NEC data were up-sampled in the same manner to a prevalence of 8%, thereby matching the expected prevalence of the disease in NICU patients [1].

Neural network models were constructed to categorize the labelled samples as either healthy or diseased with NEC based solely on the normalized collected spectra as model inputs. The first model was trained on the whole spectrum, while subsequent models took only the relevant feature selected wavelengths as inputs. All models were comprised of fully connected sequential networks consisting of rectified linear units (ReLu) activation functions at each layer, except for at the output which implemented a sigmoid function. Binary cross-entropy was used for loss minimization with an Adam optimizer. The training was run leveraging early stopping with patience. The models were primarily evaluated on their classification accuracy with sensitivity and specificity calculated as additional metrics for comparison.

## 2.3 | Multivariate Analysis for Feature Selection

Although a comprehensive evaluation of the entire spectrum from a moderately expensive spectrometer is effective for NEC detection, it may not be necessary. To test this hypothesis, a small number of key wavelengths with high diagnostic performance need to be determined. Moreover, a mechanistically informed neural network classifier with a limited number of inputs is less adversely affected by overfitting, which diminishes a model's applicability in real-world scenarios. It is recognized that the peaks and valleys within spectra shift and attenuate based on the chemical composition of tissue structures due

to the differences in the absorption and scattering of light by the tissue. This information provides specific characteristics within the spectra to investigate for feature selection. Thus, it is hypothesized that focusing on analysis of peaks and valleys within the data will enable the identification of a robust set of features, selected using machine learning, with high diagnostic performance.

MATLAB was employed for the automated detection of peak and valley locations in the preprocessed data. The features of wavelength and intensity ($I$ as a function of wavelength) were extracted for both peaks and valleys, thus resulting in four isolated categories: (1) peak wavelength, (2) valley wavelength, (3) peak intensity, and (4) valley intensity. Data screening excluded any feature that was not present in over 50% of all spectra. In cases where a peak or valley was absent for a given spectrum, instead of discarding the scan, the Winsorization method was applied, assigning the 2.5th percentile value of the wavelengths observed across all spectra to the individual scan [17]. This resulted in 10 features for each of the four categories.

Herein an iPCA framework was devised and implemented, to determine a lower number of diagnostic and synergetic spectral features. This selection process aims to choose a panel of features with high individual diagnostic performance and low inter-feature correlation. Unlike traditional principal component analysis (PCA) which remaps the entire dataset to a reduced number of features for dimensionality reduction, iPCA maps $n$ features to a n-dimensional vector space, ensuring each dimension is orthogonal, prior to running linear classification, with performance assessed by area under the curve (AUC). Thus, a higher AUC suggests that given the input features, a high data variance is captured, in addition to high diagnostic ability, which produces improved result. Hence, features with high diagnostic value but which maintain a low correlation with each other should capture higher data variance, thereby resulting in a higher AUC and thus are identified as key model inputs.

The proposed iPCA algorithm workflow takes place in two tiers. In each of the four data sorted categories, all combinations of three features were PCA transformation prior to performing centroid-based classification. The combination presenting the highest AUC value within each category was compiled into a "first-order model" list, resulting in a list of 12 features. When presenting these features to the updated neural network model, the number decreased to a list of 11 wavelengths of import due to redundancy within the intensity and the location features, both of which contained the same specific significant wavelength to the model.

At the second tier, the 12 first-order selected features were further reduced to a second-order panel of 7 features. This was done to determine the minimal set of features yielding the highest AUC among these selected features. This process followed a decision tree-like approach. All combinations of three features from the pool were analyzed in the same way as in tier one, and the combination producing the highest AUC was selected. Then, one by one each remaining feature was added to this initial selection, an updated AUC was calculated, and the added feature presenting the highest updated AUC was removed from the pool and kept in the selection group. This process continued until no substantial increase in AUC was observed, resulting in the list of selected features for the second-order model.

## 3 | Results

### 3.1 | iPCA Feature Selection

Spectra collected from the same infant presented robust and repeatable performance over time. The average intensity and standard deviation of 232 normalized spectra collected from a single infant over time are illustrated in Figure 3 by a solid black line and grey shading, respectively. This plot demonstrates the reliable performance of the proposed handheld device in capturing spectral information.

The evaluation of the results obtained by the proposed iPCA process are presented in Figure 3b. Furthermore, this figure illustrates that while this approach progressively reduces the number of features in the data, classification of these features with the nearest centroid classifier produces a progressively higher AUC. Nearest centroid classification of the initial group of 40 features within a three component PCA mapping presented an AUC of 0.735. The first-order group, comprising 12 features, resulted in an AUC value of 0.76. The second-order group of seven features achieved an enhanced AUC of 0.807. These results demonstrate that our proposed iPCA approach can effectively distinguish small number of characterizing features from a large group, resulting in panel of markers with high diagnostic performance and large informational variance.

Consequently, it is expected that iPCA consistently identifies and prioritizes features characterized by diminished inter-feature correlation or heightened label correlation. The correlation analysis depicted in Figure 3c supports this hypothesis, revealing a moderately low inter-feature correlation among the selected features used for classification. Figure 3d demonstrates an overall moderate univariate diagnostic performance for these features. It is noted that these results indicate that features $I$ (1442 nm) and 1800 nm exhibit lower univariate AUC values than the other five features. Intriguingly, these two features also demonstrate the lowest overall cross-correlation with other features. This example further affirms the hypothesis that iPCA selects features based on high univariate diagnostic performance and low cross-correlation, contributing to the development of a synergistic panel of markers. Furthermore, the AUC improvement demonstrated in Figure 3b confirms the effectiveness of these features in capturing crucial diagnostic data.

### 3.2 | Neural Network Modeling

The initial neural network classification model was trained on the whole collected spectrum, employing 2001 wavelengths, and presented an accuracy of 89.74%, a sensitivity of 39.23%, a specificity of 93.54%, and a precision of 31.31%. This indicated the potential for detecting NEC cases within a population with low disease prevalence, underscoring the clinical viability of the proposed diagnostic method. Following iPCA, the wavelengths determined as key features were employed

for the creation of an 11-wavelength first-order model, a 7-wavelength second-order model (507, 760, 970, 1077, 1442, 1657, and 1800 nm), and a single-wavelength model. The resulting metrics of accuracy, sensitivity, specificity, and precision for each model are presented in Table 1. It is noted that precision is low for all models, illustrating a high prevalence of false positives.

Given the reduction in model inputs, a relatively consistent accuracy was observed, not considering the single-wavelength model which was used as a baseline. There was a marginal reduction in accuracy from 89.74% to 87.74% for the first-order model and 87.49% for the second-order model. It should be noted that, due to the distribution of the data, simply predicting a healthy label would present an accuracy of 92%. Thus, sensitivity and specificity were included to indicate how well models performed at predicting NEC and healthy classes, respectively.

Though the second-order model has far fewer inputs than this whole-spectrum model, there is minimal cost to the model metrics, indicating that it is plausible to effectively run a classification

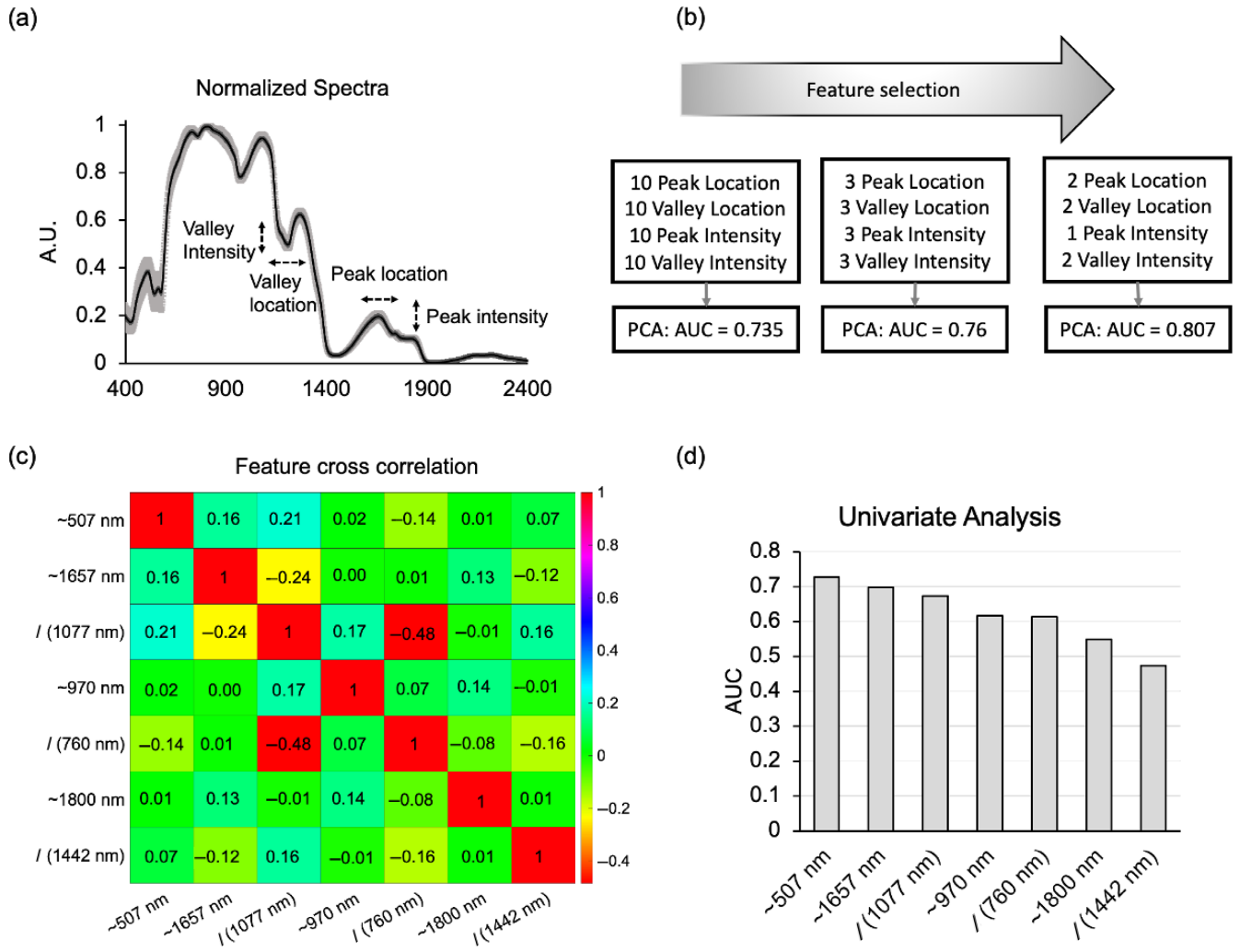


**FIGURE 3** | (a) Normalized data of 232 scans from a healthy patient with mean intensity shown as a solid black line and standard deviation shown in grey. (b) iPCA workflow for feature selection, resulting in enhanced diagnostic performance demonstrated by an increase in AUC. (c) Correlation matrix for the seven iPCA selected features showing low cross-correlation. (d) Univariate AUC values for each of the seven second-order selected features.

**TABLE 1** | Neural network validation metrics for each model.

| | Accuracy (%) | Sensitivity (%) | Specificity (%) | Precision (%) |
|---|---|---|---|---|
| Whole-spectrum model | 89.74 | 39.23 | 93.54 | 31.31 |
| First-order model | 87.74 | 89.28 | 87.83 | 35.20 |
| Second-order model | 87.49 | 42.85 | 90.85 | 26.03 |
| Single-wavelength model | 70.04 | 71.49 | 69.93 | 15.18 |

model using a small number of iPCA identified features. Though the second-order model had a higher AUC than the first-order model when using the centroid-based classifier, and the whole-spectrum model provided more data for analysis, the first-order model demonstrated the highest sensitivity by a large margin at 89.28%. This indicates that the majority of diseased cases were correctly classified by this model. Overall, the evaluation of this clinical data provides proof of concept regarding the feasibility of detecting NEC using spectral analysis.

## 4 | Discussion

The most familiar applications of clinical spectroscopy are commercially available devices such as pulse oximeters that provide a quantitative measurement of tissue or blood oxygen saturation [16]. Attempts to detect NEC have been with limited success and have not led to real-world practice changes [18, 19]. Oxyhemoglobin, however, is just one of dozens of biological chromophores, or light-absorbing molecules. Accordingly, for full characterization of organs in complex disease states, such as ischemia or cancer, in which the cellular pathways are incompletely understood, we suggest a qualitative approach is required. This is the first work, to our knowledge, to use a purely empirical approach to distinguish NEC disease among infants. This builds on work that has demonstrated that ischemic tissues have identifiable changes in their spectral intensity, though never previously performed on cavitary organs in a non-invasive fashion [20]. We utilized a variety of machine learning techniques to analyze the spectroscopy data, achieving high accuracy in distinguishing between abnormal cases susceptible to NEC and healthy controls in infants. Importantly, the detected spectroscopic signals herein are a result of backscattered signals, absorption, and, to a small degree, autofluorescence, without fluorescent contrasts or dyes that are being developed in other contexts. Hence, we opted for this label-free spectroscopic screening approach based on the premise that variations in tissue structure and composition, underlying infants' thin skin, modify the spectroscopic signature of respective disease, thereby altering signals.

We demonstrated the proof of concept that neural networks can distinguish NEC with a high accuracy of 89.74% (sensitivity = 39.23%, specificity = 93.54%). The higher specificity compared to the lower sensitivity is a consequence of the imbalanced dataset, with a notably low disease prevalence. The low disease prevalence limitation was partially addressed by up sampling disease-labelled data for training and evaluation of our approach. We aimed to develop mechanistically driven neural network models, since variations in the intensity and wavelength of spectra extrema are associated light's interaction with changes in tissues composition. To achieve this, a novel iPCA analysis was utilized to identify a small panel of wavelengths highly relevant to the detection of NEC disease. Using these selected features for neural network modeling showed a minimal reduction (less than 2.5%) in model accuracy based on only 11 (first-order reduction) or 7 spectra (second-order reduction) in comparison with the full 2001 spectra. Though there was a similar small reduction in specificity, there was a notable increase in sensitivity to the disease, with a ~50% increase from the whole-spectrum model to the first-order model. This demonstrates the value of using a mechanistically driven approach for feature selection.

Due to the increase in AUC between the first- and second-order panels of selected features, one might expect a similar result for performance of the corresponding neural network models. It should be noted that unlike the nearest centroid classifier, which implements a linear function for classification, a neural network can determine a functional separator of arbitrary shape. Therefore, more inputs will likely present a more accurate prediction of the classifier, thus improving model performance in general. It has been shown that a reduction in the number of model input features can result in reduced model overfitting, which occurs when models learn from noise or irrelevant patterns in the data. As a result of overfitting, a model may not generalize well from training data to unseen test data. Though there is an informational loss when removing features from the data, by using a subset of features, redundant information and excessive noise may be removed, thereby enabling better generalizability. Furthermore, by removing redundant information, multicollinearity and model inefficiencies are removed enabling more accurate determination of model weights.

A drawback of this study includes a limited number of patients and specifically a low number of patients with NEC, which resulted in a large data imbalance between classes. This increases model uncertainty and makes neural network model training more difficult to do without introducing bias. Though this is limited to an empirical analysis, further analysis can be done to determine the limitations of the technology with regards to factors such as subject skin thickness or weight limitations that may prevent effective measurement of organs through the abdominal wall. Additionally, skin tone was not rigorously studied in this work, but all Fitzpatrick skin types are represented in this patient cohort. Furthermore, the device limitations can be explored through phantom experiments and theory-based simulations relevant to this experimental configuration. In future development of this work, it is recommended that multiple scans are collected at each period of acquisition, which can easily be done due to the negligible time and cost associated with capture most data. This will help offset the data imbalance problem and enable greater model accuracy in the future.

In future work, further investigation should be conducted to determine the significance of the selected feature wavelengths as this may provide insight into the underlying biological mechanism of the disease. For instance, spectral variations at ~1800 nm are known to correlate with changes in C—H composition [21]. The variation at ~1657 nm potentially arises from CH stretching of methyl group in carbohydrates and lipids in tissue beneath the skin [22]. Spectral variation in ~1442 nm can be due to variation in $H_2O$, CH, ROH, $CONH_2$, or CONHR [21]. Spectral variations at ~970 nm are associated with CH or $H_2O$, as indicated in the literature [21]. It is noted that there are challenges associated with precisely determining tissue composition; however, this endeavor can provide valuable insights when successful.

The high accuracy, sensitivity, and specificity of the first-order model indicates that the model is effective at identifying the

presence of disease; however, the low precision scores indicate a high false-positive rate. This is likely a result of the imbalanced dataset. Though the model overestimates the presence of disease, due to the technology's speed, low cost, and noninvasive nature it still poses an opportunity as a screening tool. In future work this low precision can be improved by increasing the diseased data set for training or by taking multiple scans for a single diagnostic instance (which poses minimal extra cost), as has been illustrated on an alternate BOS data set in Figure S1.

Building from this analysis, models should be further developed to increase diagnostic metrics. Prior to deployment in a medical setting, this can be done by conducting this analysis on a larger clinical population to validate the success and investigate the specific limitations of this technology as a NEC early detection method. Furthermore, this research focused on implementing this technology specifically for NEC; however, it may also have value for other diseases with similar characteristics which allow for data to be collected in the same manner. Additionally, there is a technical engineering opportunity presented. Given the panel of selected wavelengths, can a cheap wearable device be produced allowing for continuous patient monitoring, rather than using more expensive optical equipment which greatly exceeds the needs of the application, making it disproportional for the task at hand.

## 5 | Conclusion

This empirical research aimed to investigate the ability of BOS to detect NEC disease states in a neonatal infant clinical pilot study. It was demonstrated that NEC can be categorized from a single spectral scan using a neural network model. Deploying iPCA resulted in two panels of selected features with high AUC and low cross-correlation. These panels were each implemented in new neural network models yielding similar model metrics compared to the whole-spectrum model, with a fractional number of inputs. Although a whole spectrum provided the highest accuracy, the value of feature selection using iPCA was successfully illustrated. The selected discrete wavelengths can be utilized as key points of interest in future research. Furthermore, research should be conducted to further develop this technology to deploy it for point of care medical diagnosis.

### Author Contributions

S.D.G. directed the project and led data collection efforts. E.F., A.D., V.B., and S.D.G. contributed to conceptualization, study design, and analyses. E.F. and A.D. were responsible for designing and conducting statistical analyses, machine learning, and artificial intelligence techniques, with input from other authors. E.F., A.D., and S.D.G. drafted the manuscript, with all authors contributing to its writing, review, and editing. E.F. and A.D. contributed equally to this research.

### Acknowledgments

This research was supported by a grant from The Gerber Foundation. Additional support made possible by the National Institutes of Health Grants (NIH) grants U54CA268084, R01CA228272, and R01CA225002, National Science Foundation grant (NSF) Grant EFMA-1830961, and philanthropic support from Rob and Kristin Goldman and the Christina Carinato Charitable Foundation.

### Conflicts of Interest

The authors declare no conflicts of interest.

### Data Availability Statement

The data that support the findings of this study are available on request from the corresponding author. The data are not publicly available due to privacy or ethical restrictions.

### References

1. J. Neu and W. A. Walker, "Necrotizing enterocolitis," *New England Journal of Medicine* 364, no. 3 (2011): 255–264, https://doi.org/10.1056/NEJMra1005408.

2. D. J. Scheese, C. P. Sodhi, and D. J. Hackam, "New Insights Into the Pathogenesis of Necrotizing Enterocolitis and the Dawn of Potential Therapeutics," *Seminars in Pediatric Surgery* 32, no. 3 (2023): 151309, https://doi.org/10.1016/j.sempedsurg.2023.151309.

3. S. Al-Hamad, D. J. Hackam, S. D. Goldstein, T. A. G. M. Huisman, K. Darge, and M. Hwang, "Contrast-Enhanced Ultrasound and Near-Infrared Spectroscopy of the Neonatal Bowel: Novel, Bedside, Noninvasive, and Radiation-Free Imaging for Early Detection of Necrotizing Enterocolitis," *American Journal of Perinatology* 35, no. 14 (2018): 1358–1365.

4. E. Agakidou, C. Agakidis, H. Gika, and K. Sarafidis, "Emerging Biomarkers for Prediction and Early Diagnosis of Necrotizing Enterocolitis in the Era of Metabolomics and Proteomics," *Frontiers in Pediatrics* 8 (2020): 602255, https://doi.org/10.3389/fped.2020.602255.

5. M. K. Syed, A. A. Al Faqeeh, N. Saeed, et al., "Surgical Versus Medical Management of Necrotizing Enterocolitis With and Without Intestinal Perforation: A Retrospective Chart Review," *Cureus* 13, no. 6 (2021): e15722, https://doi.org/10.7759/cureus.15722.

6. A. J. Thompson, S. Coda, M. B. Sørensen, et al., "In Vivo Measurements of Diffuse Reflectance and Time-Resolved Autofluorescence Emission Spectra of Basal Cell Carcinomas," *Journal of Biophotonics* 5, no. 3 (2012): 240–254, https://doi.org/10.1002/jbio.201100126.

7. R. J. Beaulieu, S. D. Goldstein, J. Singh, B. Safar, A. Banerjee, and N. Ahuja, "Automated Diagnosis of Colon Cancer Using Hyperspectral Sensing," *International Journal of Medical Robotics and Computer Assisted Surgery* 14, no. 3 (2018): e1897, https://doi.org/10.1002/rcs.1897.

8. S. Chakravarti, S. Srivastava, and A. J. C. Mittnacht, "Near Infrared Spectroscopy (NIRS) in Children," *Seminars in Cardiothoracic and Vascular Anesthesia* 12, no. 1 (2008): 70–79, https://doi.org/10.1177/1089253208316444.

9. L. Finlayson, I. R. M. Barnard, L. McMillan, et al., "Depth Penetration of Light Into Skin as a Function of Wavelength From 200 to 1000 nm," *Photochemistry and Photobiology* 98, no. 4 (2022): 974–981, https://doi.org/10.1111/php.13550.

10. L. A. Sordillo, Y. Pu, S. Pratavieira, Y. Budansky, and R. R. Alfano, "Deep Optical Imaging of Tissue Using the Second and Third Near-Infrared Spectral Windows," *Journal of Biomedical Optics* 19, no. 5 (2014): 056004, https://doi.org/10.1117/1.JBO.19.5.056004.

11. I. M. F. de Souza, G. L. N. Vitral, M. V. Caliari, and Z. S. N. Reis, "Association Between the Chronology of Gestation and the Morphometrical Skin Characteristics at Childbirth: A Development of Predictive Model," *BMJ Health and Care Informatics* 28, no. 1 (2021): e100476, https://doi.org/10.1136/bmjhci-2021-100476.

12. G. L. N. Vitral, R. A. P. L. Aguiar, I. M. F. de Souza, M. A. S. Rego, R. N. Guimaraes, and Z. S. N. Reis, "Skin Thickness as a Potential Marker of Gestational Age at Birth Despite Different Fetal Growth Profiles: A Feasibility Study," *PLoS One* 13, no. 4 (2018): e0196542, https://doi.org/10.1371/journal.pone.0196542.

13. L. Kakasheva-Mazhenkovska, L. Milenkova, G. Gjokik, and V. Janevska, "Variations of the Histomorphological Characteristics of

Human Skin of Different Body Regions in Subjects of Different Age," *Prilozi* 32, no. 2 (2011): 119–128.

14. S. D. Goldstein, R. J. Beaulieu, D. F. Niño, et al., "Early Detection of Necrotizing Enterocolitis Using Broadband Optical Spectroscopy," *Journal of Pediatric Surgery* 53, no. 6 (2018): 1192–1196, https://doi.org/10.1016/j.jpedsurg.2018.02.083.

15. E. Flowerday, A. Daneshkhah, V. Backman, and S. D. Goldstein, "Application of Machine Learning Algorithms for the Classification of Organs in Premature Infants Using Broadband Optical Spectroscopy," *Advanced Chemical Microscopy for Life Science and Translational Medicine* 11973 (2022): 7–12, https://doi.org/10.1117/12.2609659.

16. S. M. Bailey and P. V. Mally, "Review of Splanchnic Oximetry in Clinical Medicine," *Journal of Biomedical Optics* 21, no. 9 (2016): 091306, https://doi.org/10.1117/1.JBO.21.9.091306.

17. J. H. Sullivan, M. Warkentin, and L. Wallace, "So Many Ways for Assessing Outliers: What Really Works and Does It Matter?," *Journal of Business Research* 132 (2021): 530–543, https://doi.org/10.1016/j.jbusres.2021.03.066.

18. I. J. Zamora, B. Stoll, C. G. Ethun, et al., "Low Abdominal NIRS Values and Elevated Plasma Intestinal Fatty Acid-Binding Protein in a Premature Piglet Model of Necrotizing Enterocolitis," *PLoS One* 10, no. 6 (2015): e0125437, https://doi.org/10.1371/journal.pone.0125437.

19. T. E. Schat, M. Schurink, M. E. van der Lann, et al., "Near-Infrared Spectroscopy to Predict the Course of Necrotizing Enterocolitis," *PLoS One* 11, no. 5 (2016): e0154710, https://doi.org/10.1371/journal.pone.0154710.

20. H. Akbari, Y. Kosugi, K. Kojima, and N. Tanaka, "Detection and Analysis of the Intestinal Ischemia Using Visible and Invisible Hyperspectral Imaging," *IEEE Transactions on Biomedical Engineering* 57, no. 8 (2010): 2011–2017, https://doi.org/10.1109/TBME.2010.2049110.

21. A. Currà, R. Gasbarrone, A. Cardillo, et al., "Near-Infrared Spectroscopy as a Tool for In Vivo Analysis of Human Muscles," *Scientific Reports* 9, no. 1 (2019): 8623, https://doi.org/10.1038/s41598-019-44896-8.

22. H. R. Jarski, D. R. Groom, and T. D. McGillivray, "Use of NIR Spectroscopy for On-Site Betaine Measurement in the ACS Hillsboro Molasses Desugarization Plant," 2009, in *Proceedings of 35th Biennial Meeting*, ASSBT, https://doi.org/10.5274/ASSBT.2009.58.

## Supporting Information

Additional supporting information can be found online in the Supporting Information section.